SISTEMAS ESTELARES

Material didáctico para las clases de "*Escala de distancias extragaláctica*"

Clases teóricas dictadas por:
Dra. Lilia P. Bassino

Relación P-L de Cefeidas clásicas (o Tipo I): "Leavitt Law"

Tammann et al. 2008,
ApJ 679, 52

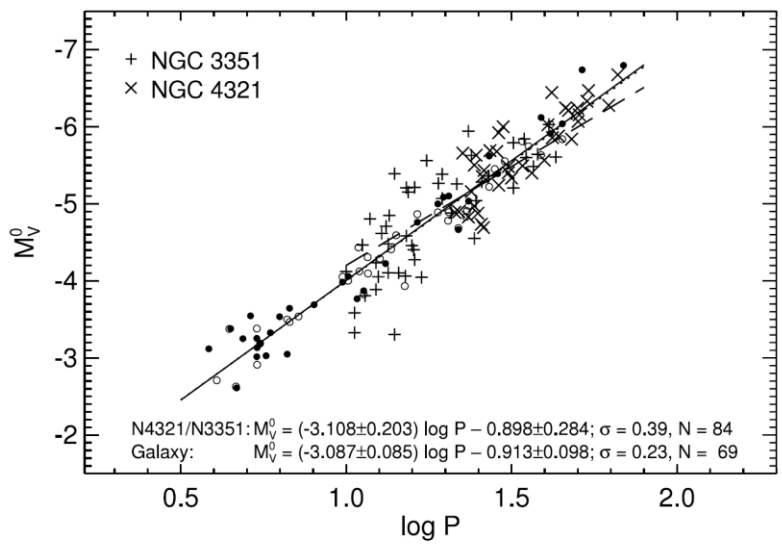

FIG. 2.—*P-L* relation in *V* of metal-rich Cepheids in the Galaxy (*circles*), NGC 4321 (*crosses*), and NGC 3351 (*plus signs*). The latter two galaxies define a slope in good agreement with the Galaxy (*dotted line*). For comparison the LMC *P-L* relation for $\log P > 1.0$ is shown as a dashed line.

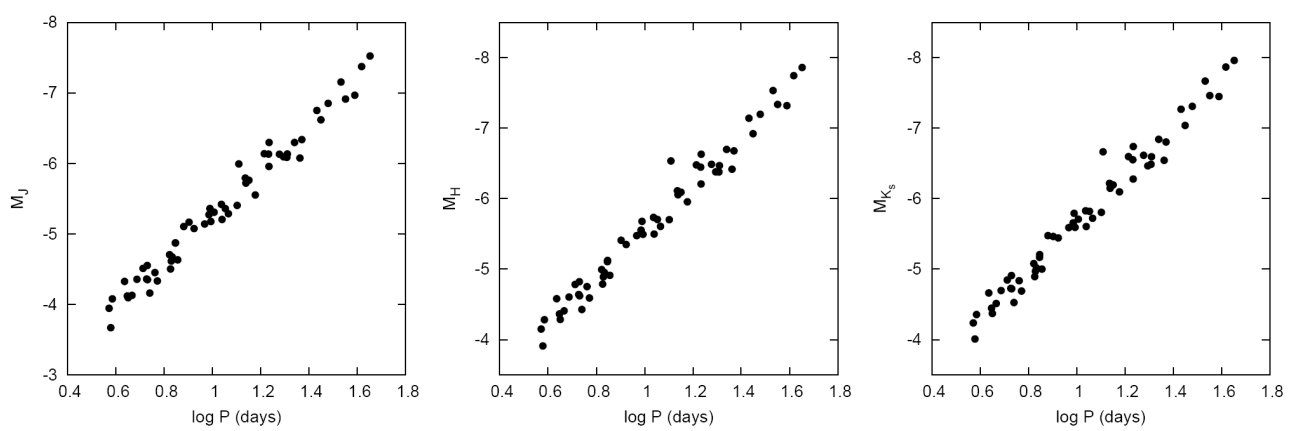

Fig. 3. Adopted Galactic *PL* relations in near-infrared bands.

Fouqué et al. 2007,
A&A 476, 73

Relación P-L de Cefeidas clásicas

Efecto de la metalicidad en Cefeidas Galácticas y de las Nubes de Magallanes:

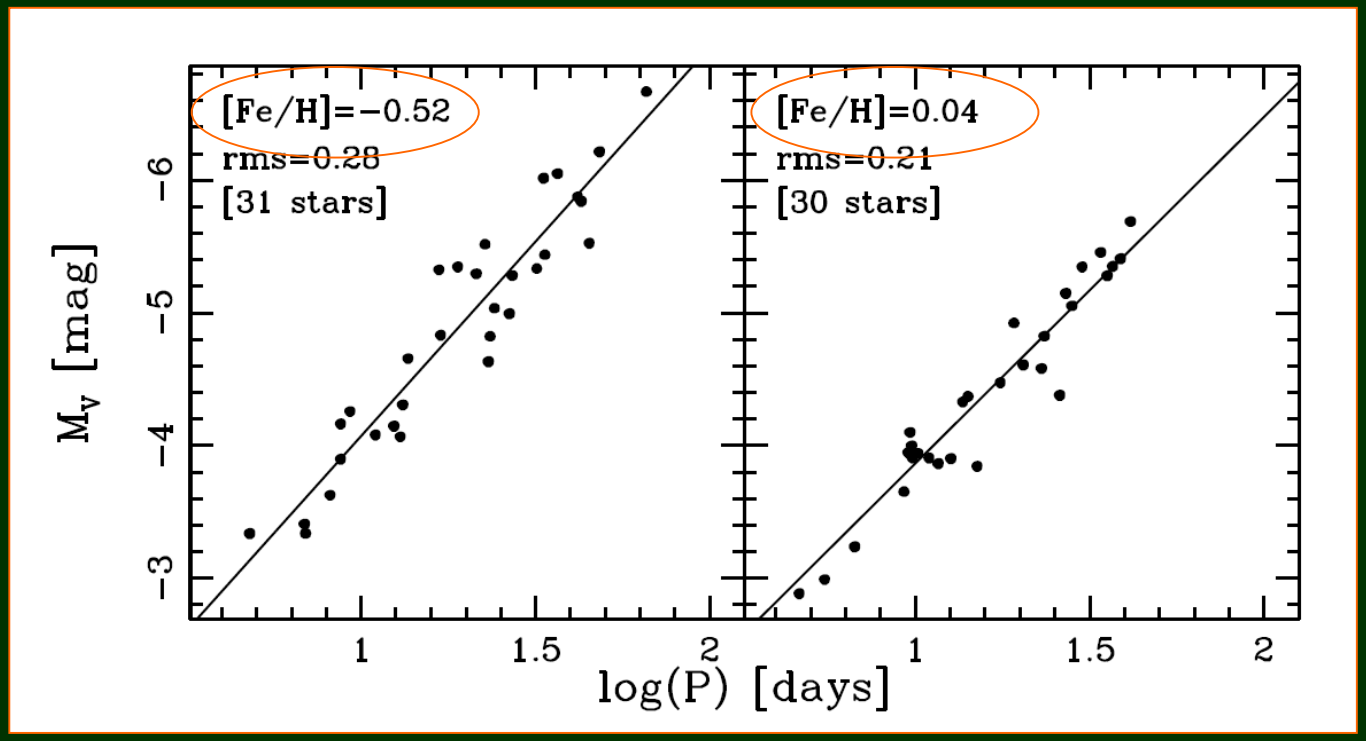

Romaniello et al. 2008,
A&A 488, 731

Relación P-L de Cefeidas clásicas en la LMC (Nube Mayor de Mag.)

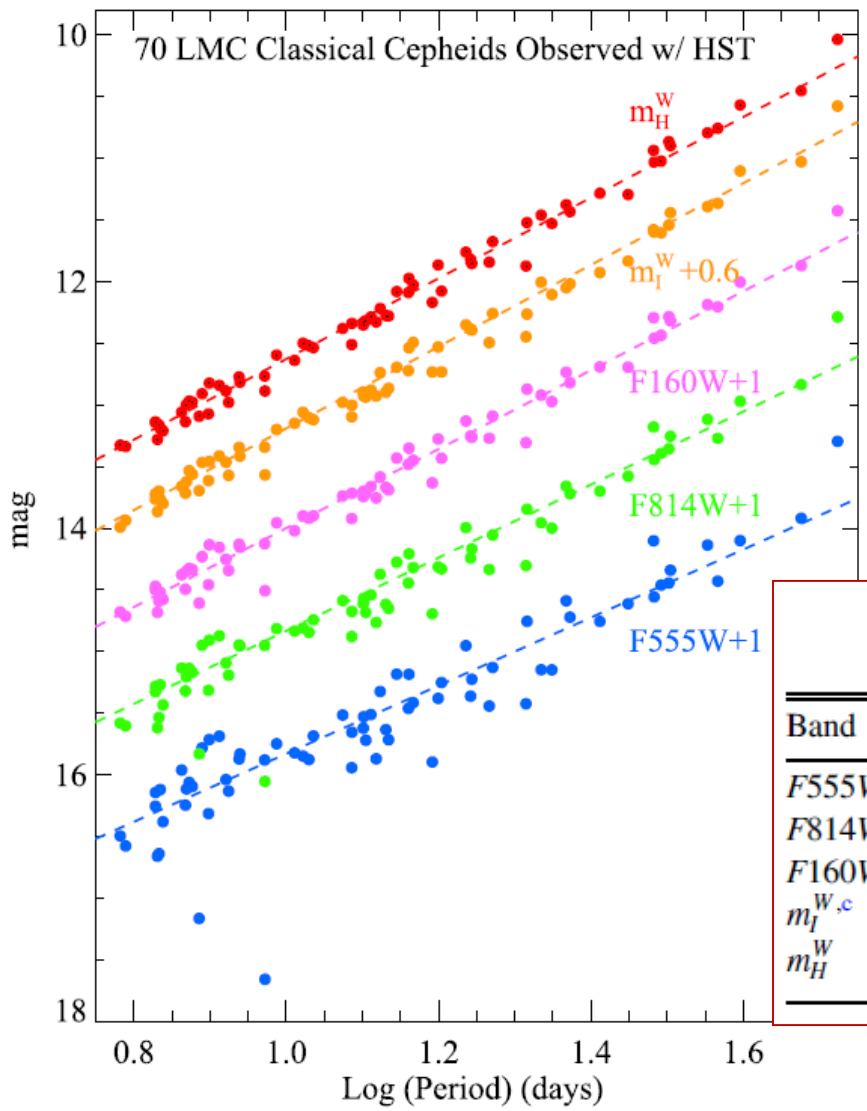

Figure 3. Period–mean magnitude relation for the 70 LMC Cepheids with slopes and statistics given in Table 3.

Filtros HST: F555W (V)
F814W (I)
F160W (H)

Table 3
Period–Mean magnitude Relations from *HST* LMC Cepheids

Band	Slope[a]	Intercept[b]	Scatter[b]
F555W	−2.76	17.638	0.312
F814W	−2.96	16.854	0.202
F160W	−3.20	16.209	0.104
$m_I^{W,c}$	−3.31	15.935	0.085
m_H^W	−3.26	15.898[d]	0.075

Riess et al. 2019,
ApJ 876, #85

Wesenheit indices, $m_H^W = m_{F160W} - 0.386(m_{F555W} - m_{F814W})$
and $m_I^W = m_{F814W} - 1.3(m_{F555W} - m_{F814W})$.

Magnitudes absolutas V de RR Lyrae

a) *RR Lyrae and HB stars. Trigonometric Parallaxes*

$$M_V(RR) = 0.18([\mathrm{Fe/H}] + 1.5) + 0.62 \pm 0.11.$$

b) *RR Lyrae and HB stars. Statistical Parallaxes*

$$M_V(RR) = 0.18([\mathrm{Fe/H}] + 1.5) + 0.73 \pm 0.12.$$

c) *RR Lyrae and HB stars. The Baade-Wesselink method.*

$$M_V(RR) = 0.18([\mathrm{Fe/H}] + 1.5) + 0.71 \pm 0.08.$$

Carretta et al. 2000,
ApJ 533, 215

Magnitud absoluta Ks (NIR) de RR Lyr: rel. P-L-metalicidad

$$\langle M_{Ks} \rangle = -0.769 + 0.088\,[Fe/H] - 2.33\,\log P$$

En el visual:

$$\langle M_V \rangle = 1.094 + 0.232\,[Fe/H]$$

- Con paralajes estadísticas, 400 RR Lyr de campo.

Dambis et al. 2013,
MNRAS 435, 3206

Relación P-L de Cefeidas Tipo II

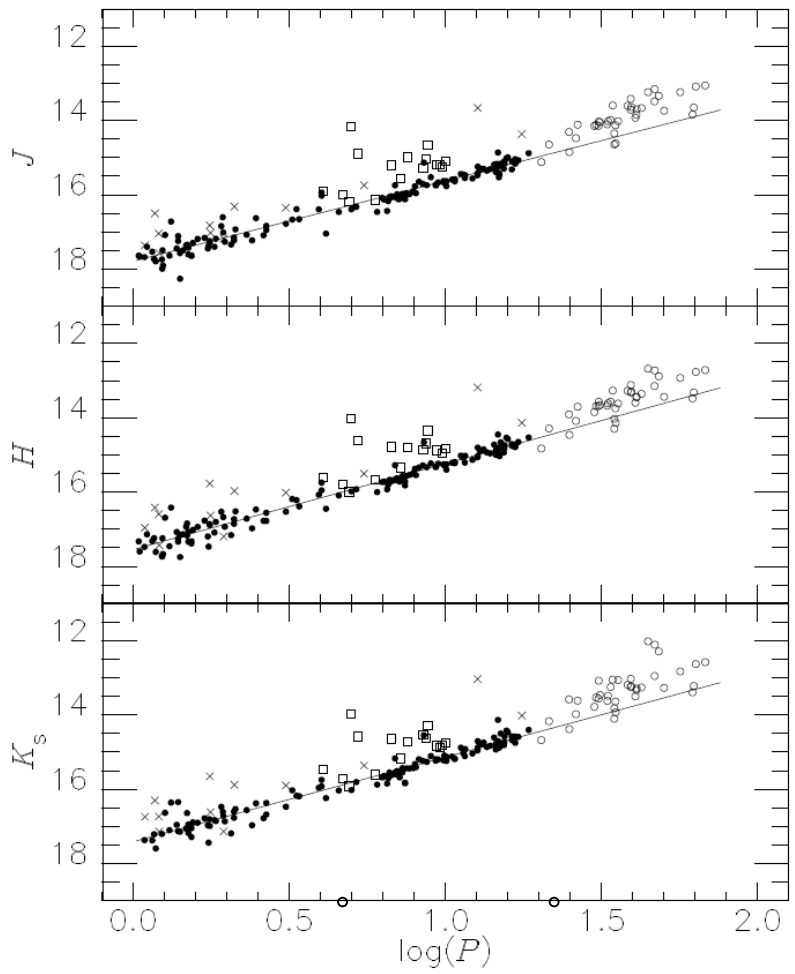

Figure 2. Period-magnitude relation of CephIIs in the LMC. The phase-corrected JHK_s magnitudes are plotted against periods. Filled circles indicate BL+WV used to solve the PL relations while crosses indicate those excluded, open squares pW, and open circles RV.

P < 4d: BL Herculis

4 < P < 20d: W Virginis

Matsunaga et al. 2009, MNRAS 397, 933

Relación M_V_máx vs. velocidad de decaimiento del brillo en Novas

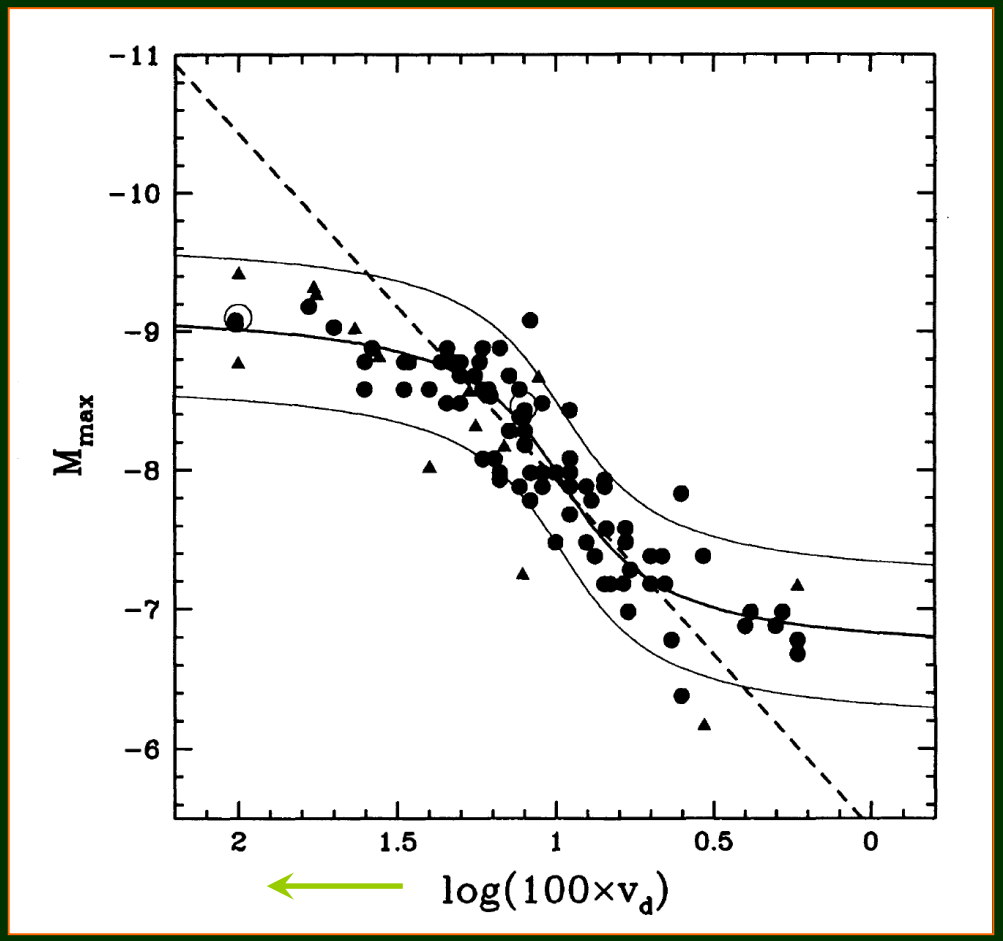

$v_d = 2 / t_2$

t_2 [días]: tiempo en que el brillo de la nova decae 2 mag por debajo del máximo.

Della Valle & Livio 1995
ApJ 452, 704

Brillo del extremo de la rama de gigantes rojas (TRGB)

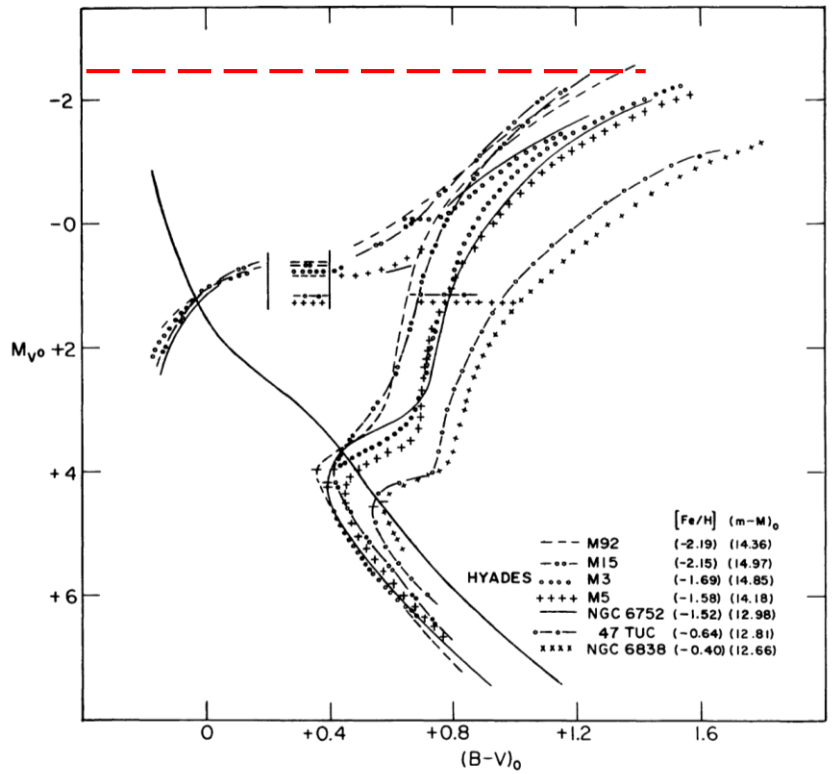

Fig. 2 The composite CMD for seven globular clusters. Note that the brightest red giant stars of the five most metal-poor clusters have very similar absolute magnitudes of about $M_V = -2.5$ (from Sandage 1986b). The I magnitude of the brightest red giants is even more stable near $M_I = -4.05$ as found by Da Costa & Armandroff (1990).

Tammann et al. 2008,
A&ARv 15, 289

DCM de la galaxia M32: TRGB

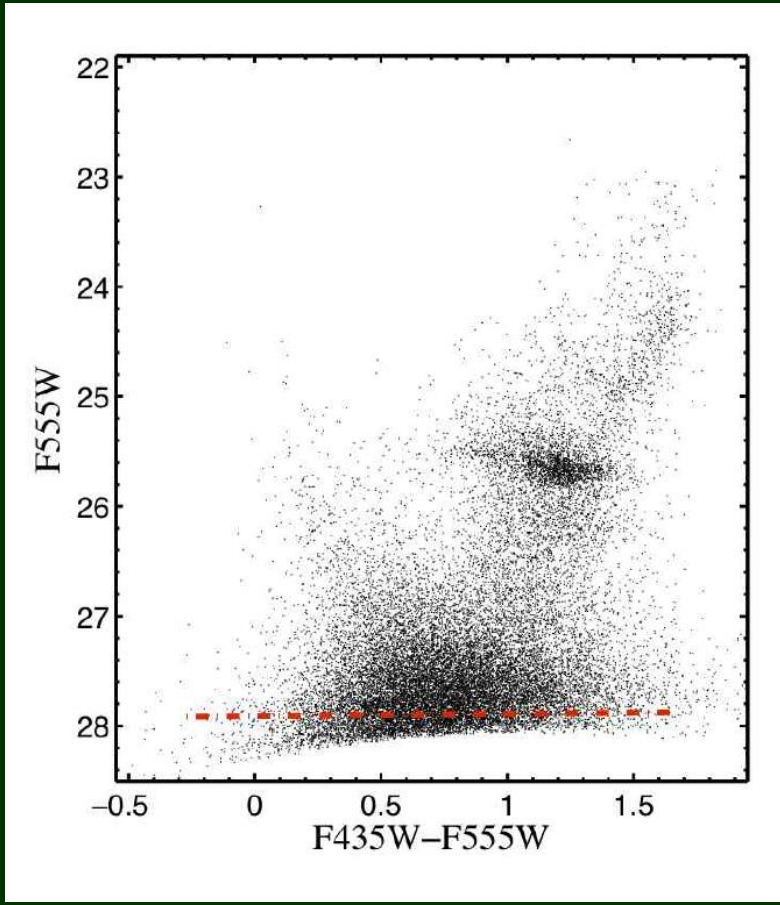

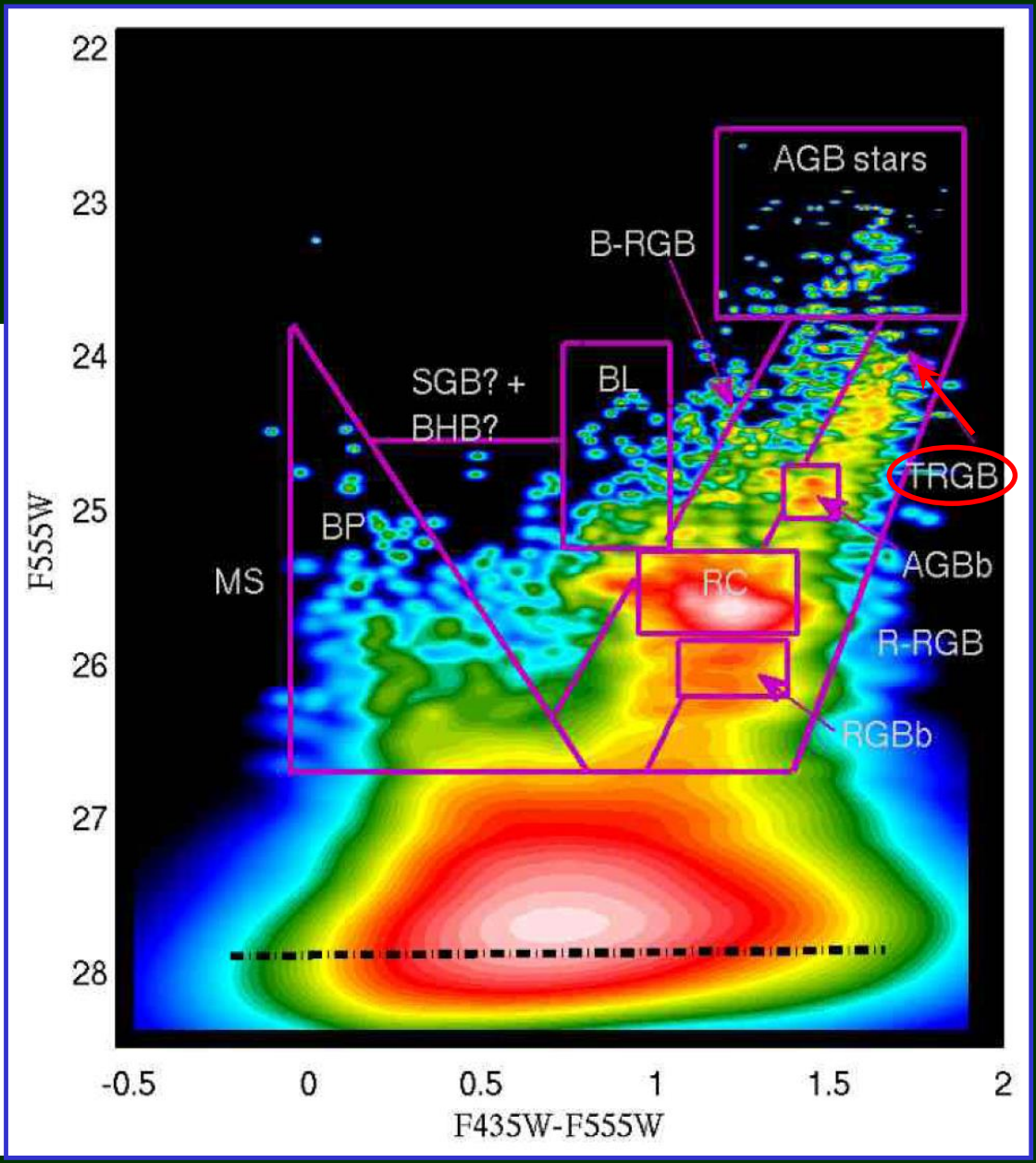

Monachesi et al. 2011, ApJ 727, 55

Relación de Tully - Fisher (TF)

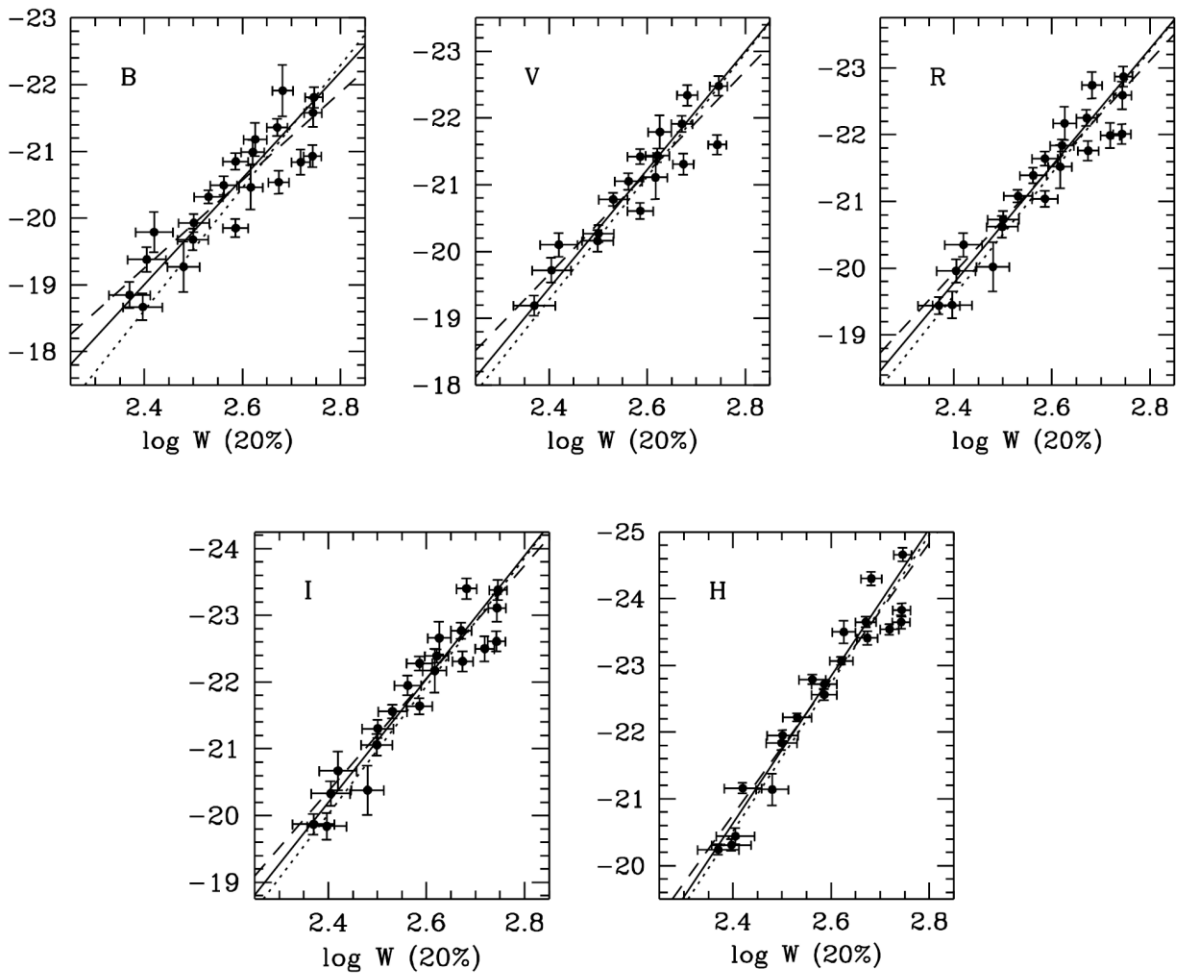

FIG. 1.—$BVRIH_{-0.5}$ Tully-Fisher relations for spiral galaxies with Cepheid distances, using 20% line width. Solid lines represent the bivariate fits, while the dotted and dashed lines represent inverse and direct fits, respectively.

Sakai et al. 2000, ApJ 529, 698
HST Key Project

Relación de

Tully - Fisher bariónica

$\mathcal{M}_* / L$ = cte (para c/tipo de gal)

➔ $\mathcal{M}_*$

$\mathcal{M}_d = \mathcal{M}_* + \mathcal{M}_{gas}$

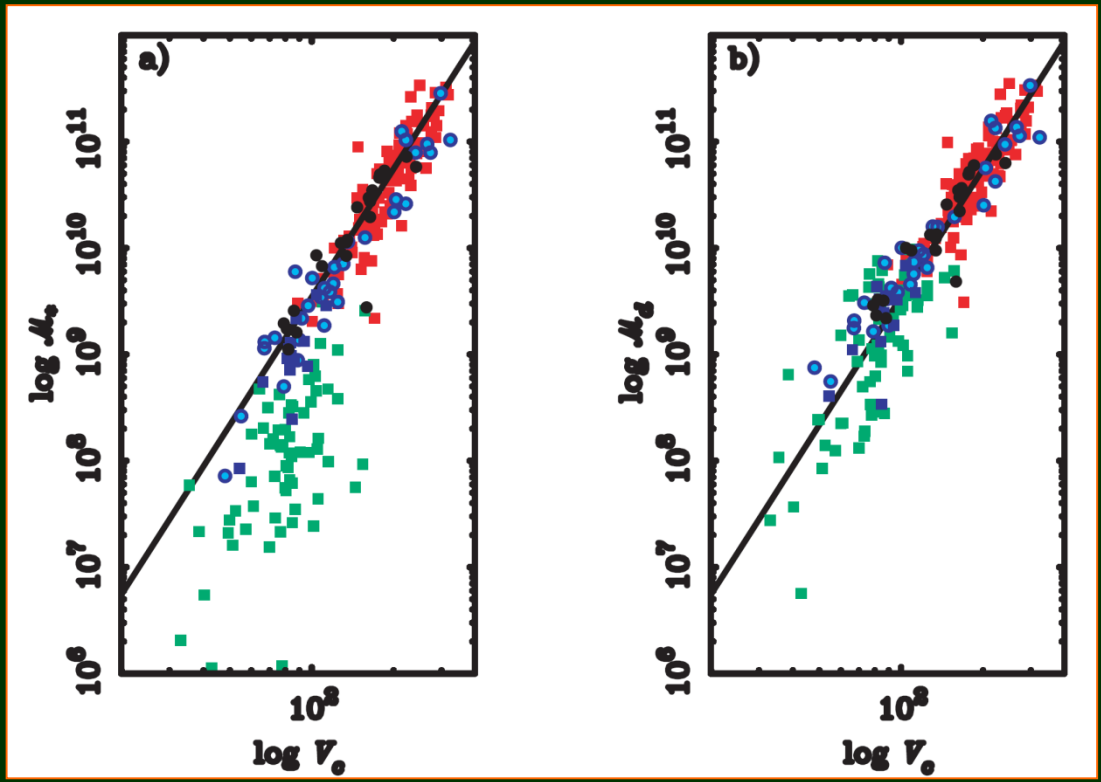

FIG. 1.—Tully-Fisher relation plotted as (*a*) stellar mass and (*b*) baryonic disk mass against rotation velocity. The squares represent galaxies where the circular velocity is estimated from the line width by $V_c = \frac{1}{2}W_{20}$, while the circles have $V_c = V_{\rm flat}$ from resolved rotation curves. The data employed include the *H*-band data of Bothun et al. (1985; *red*), the *K′*-band data of Verheijen (1997; *black*), and the *I*-band data of Pildis et al. (1997) with velocities as reported by Eder & Schombert (2000; *green*). Also shown are the *B*-band data of McGaugh & de Blok (1998; *light blue*) and of Matthews et al. (1998; *dark blue*). The stellar mass is computed from the luminosity by assuming a constant mass-to-light ratio ($M_* = \Upsilon_* L$), so (*a*) is directly analogous to the usual luminosity–line width diagram. We assume mass-to-light ratios for the stellar populations of late-type galaxies of $\Upsilon_*^B = 1.4$, $\Upsilon_*^I = 1.7$, $\Upsilon_*^H = 1.0$, and $\Upsilon_*^{K'} = 0.8\ M_\odot/L_\odot$ (see text). In (*b*), we plot the total baryonic disk mass $M_d = M_* + M_{\rm gas}$ with $M_{\rm gas} = 1.4 M_{\rm H\,I}$. In (*a*), a clear break is apparent. Galaxies with $V_c \lesssim 90$ km s^{-1} fall systematically below the Tully-Fisher relation defined by brighter galaxies. In (*b*), the deficit in mass apparent in (*a*) has been restored by including the gas mass. The solid line is an unweighted fit to the red-band data in (*b*) with a correlation coefficient of 0.92 and a slope indistinguishable from 4.

McGaugh et al. 2000,
ApJ 533, L99

Plano fundamental y relación D_n - σ (Faber - Jackson)

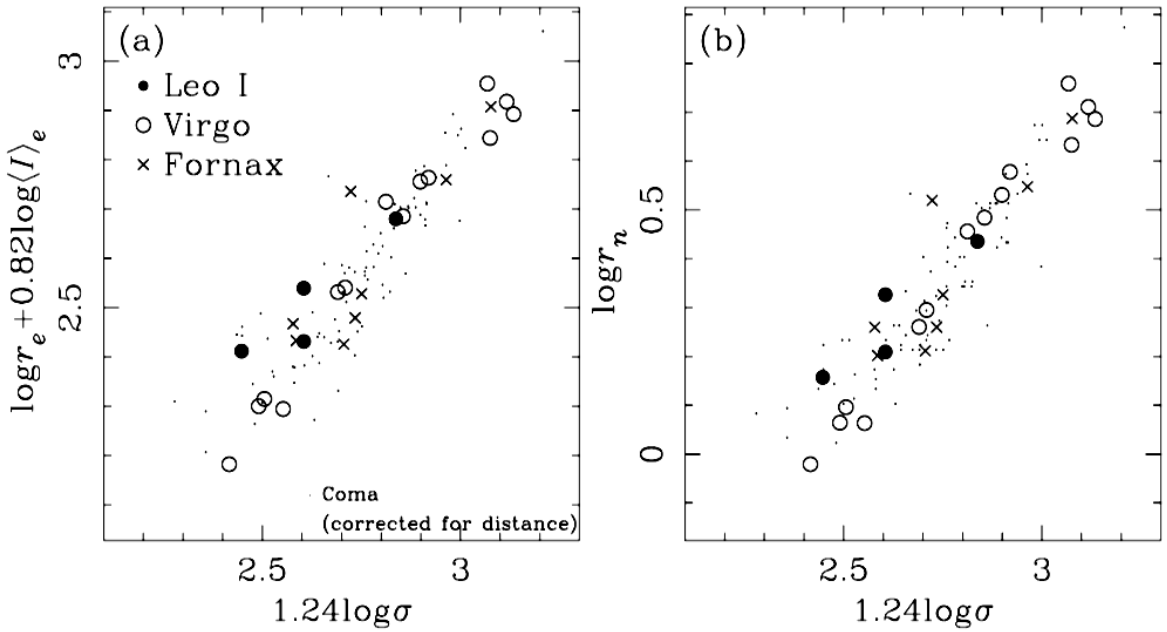

FIG. 2.—(*a*) Fundamental plane and (*b*) D_n-σ relations in Leo I, Virgo, and Fornax, where distance effects have been removed. The Coma sample from Jørgensen et al. (1995a, 1995b) is shown, corrected for distance, by small points.

r_e , r_n : [kpc]

Kelson et al. 2000, ApJ 529, 768
HST Key Project

Magnitud absoluta en el máximo de Supernovas tipo Ia (SNIa)

TABLE 4

WEIGHTED, METALLICITY-CORRECTED MEAN ABSOLUTE MAGNITUDES OF SNe Ia

Method	M_B	M_V	M_I
1. from μ^0(Gal)	−19.50	−19.47	−19.19
2. from μ^0_Z(LMC)	−19.36	−19.32	−19.07
3. from μ^0_Z(MF)	−19.48	−19.45	−19.20
4. from μ^0_Z (Paper IV)	−19.49	−19.46	−19.22
Mean of (1)–(4)	−19.46	−19.43	−19.17
Mean of (1), (3), and (4)	−19.49	−19.46	−19.20

NOTE.—The error of the mean is 0.04 mag for all entries.

Calibradas con P – L de Cefeidas

Se aplica una *corrección previa* para estandarizar la forma de la curva de luz (relación entre brillo en el máximo y forma de la curva de luz: más débiles → más empinada)

Sandage et al. 2006
ApJ 653, 843

Función de luminosidad de Nebulosas Planetarias

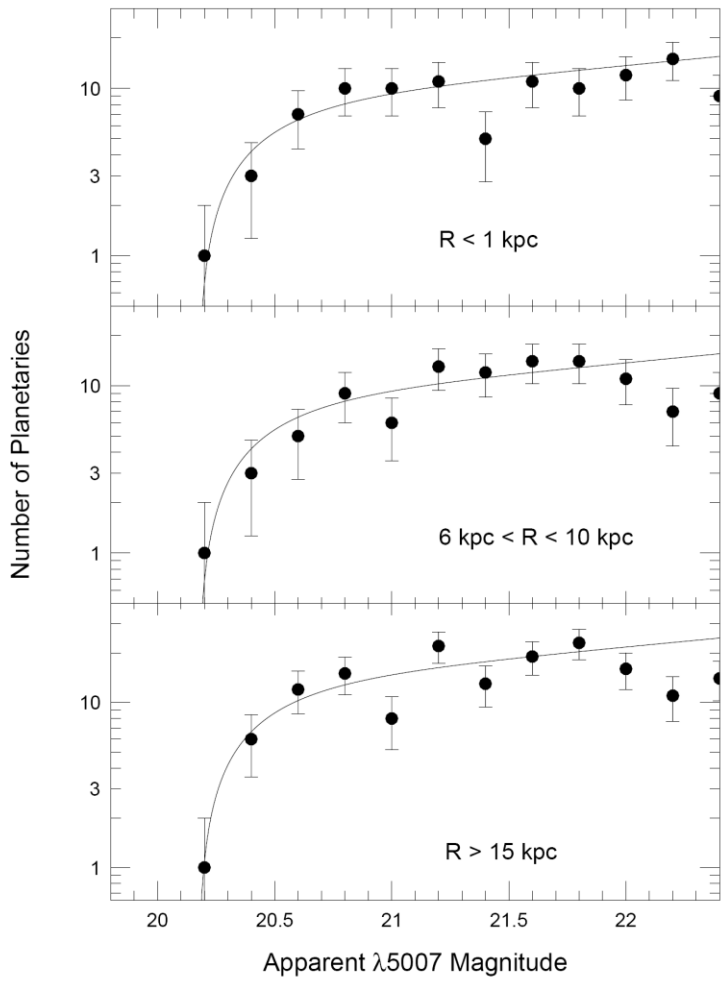

Fig. 6. The observed planetary nebula luminosity functions for samples of M31 PNe projected at three different galactocentric radii. The curves show the best-fitting empirical law. The derived PNLF distances are consisted to within ~ 0.05 mag. The turnover in the luminosity function past $m_{5007} \gtrsim 22$ in the intermediate and large-radii samples is real, and indicates the presence of relatively massive PN central stars.

Magnitud absoluta del extremo brillante de la FL ("cut-off "):

$$M(\lambda 5007) \cong -4.5 \text{ mag}$$

Ciardullo 2003,
Lecture Notes in Physics 635, 243

Función de luminosidad de Cúmulos Globulares

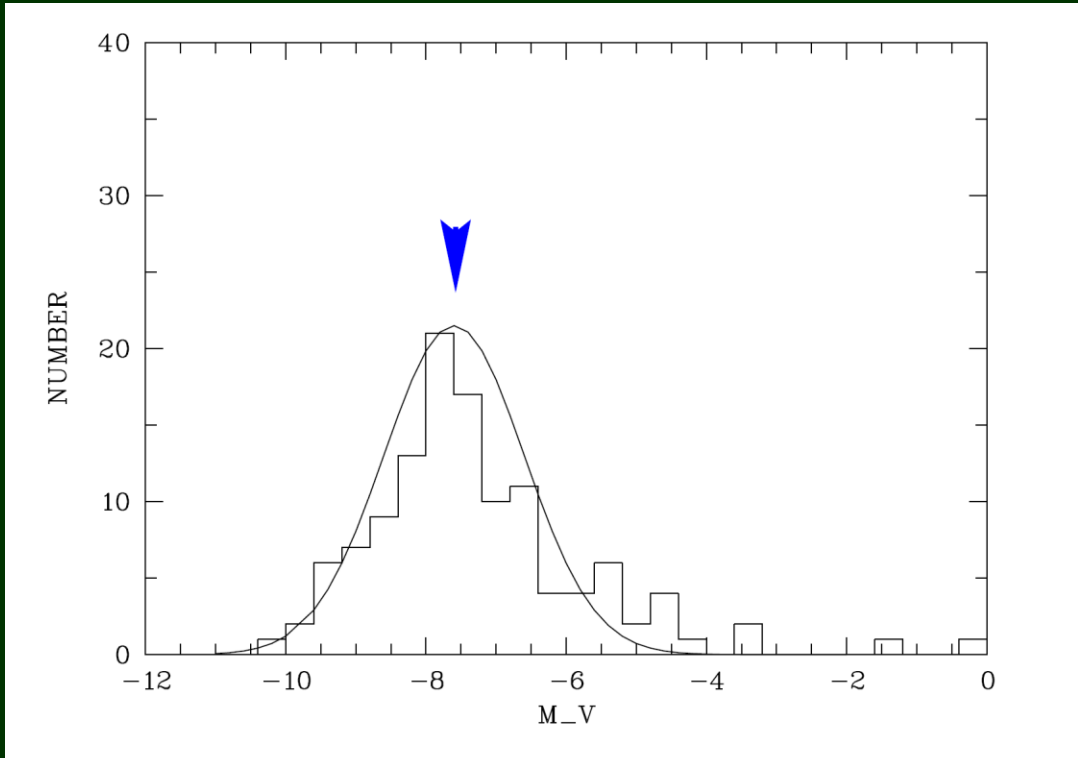

Fig. 1. The upper panel shows the globular cluster luminosity function for the galactic system together with a fitted Gaussian to the distribution.

Magnitud absoluta del máximo de la FL

(“ turn-over ”): $M_V \cong$ -7.4 mag

Richtler 2003,
Lecture Notes in Physics 635, 281

Constante de Hubble H_0

❖ En octubre de 2018, por votación de sus miembros (78% a favor), la Unión Astronómica Internacional (IAU) recomendó:

Ley de Hubble → Ley de Hubble – Lemaître

29 October 2018

IAU members vote to recommend renaming the Hubble law as the Hubble - Lemaître law

Constante de Hubble H_0

Resultado del Key Project del HST $H_0 = 72 \pm 8$ km / s Mpc
(Freedman et al. 2001, ApJ 553, 47)

Sandage, Tammann et al. 2006, $H_0 = 62.3 \pm 6.3$ km / s Mpc
ApJ 653, 843

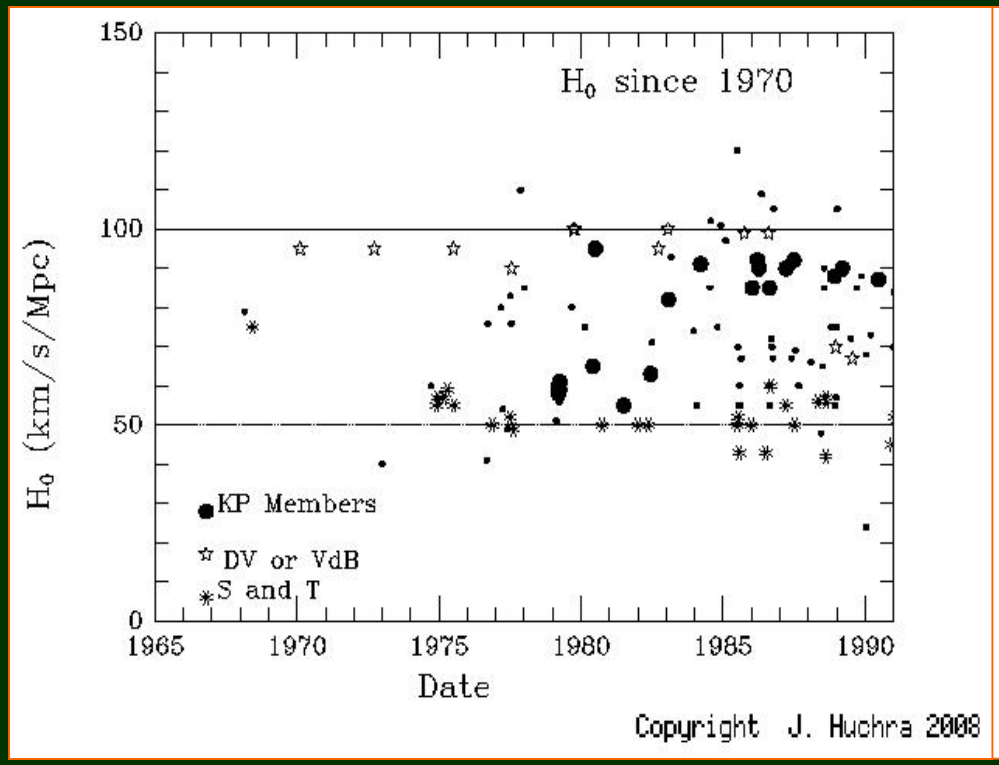

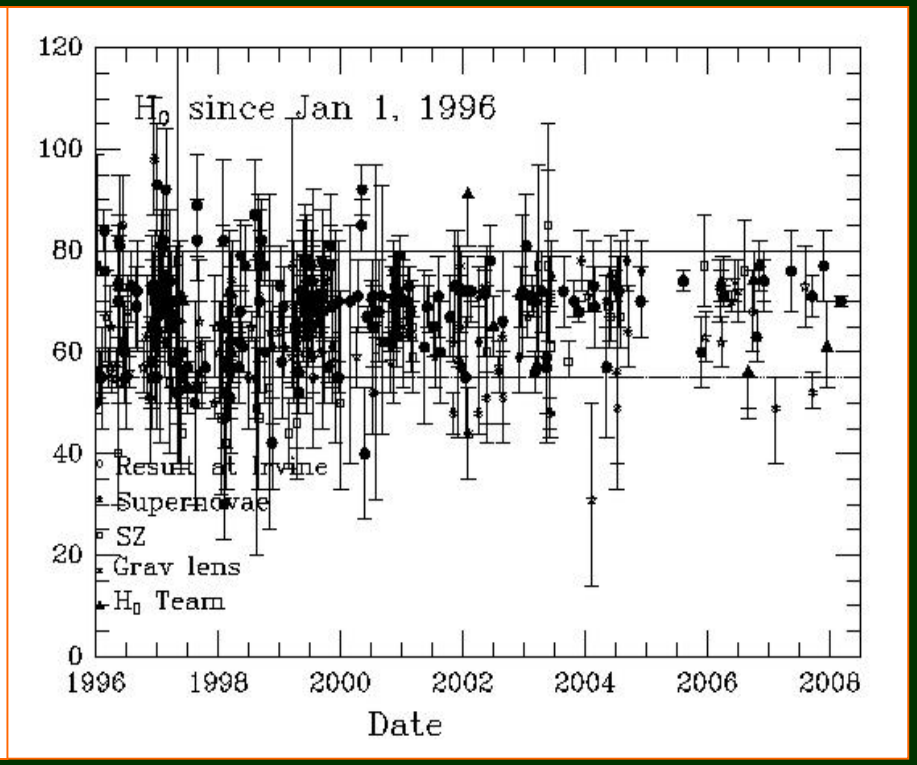

Constante de Hubble H_0

Riess et al. 2011, ApJ 730, 119 $H_0 = 73.8 \pm 2.4$ km / s Mpc (error 3.3%)

Riess et al. 2018, ApJ 861, #126 $H_0 = 73.52 \pm 1.62$ km / s Mpc (error 2.2%)

50 Cef. de la Vía Láctea, fotometría HST + paralajes Gaia DR2

Riess et al. 2019, ApJ 876, #85 $H_0 = 74.03 \pm 1.42$ km / s Mpc (error 1.9%)

70 Cef. de la LMC, fotometría HST + d LMC (bin. eclip. + SNIa)

Cefeidas en la galaxia NGC 5584 (d = 24 Mpc, SNIa en 2007)

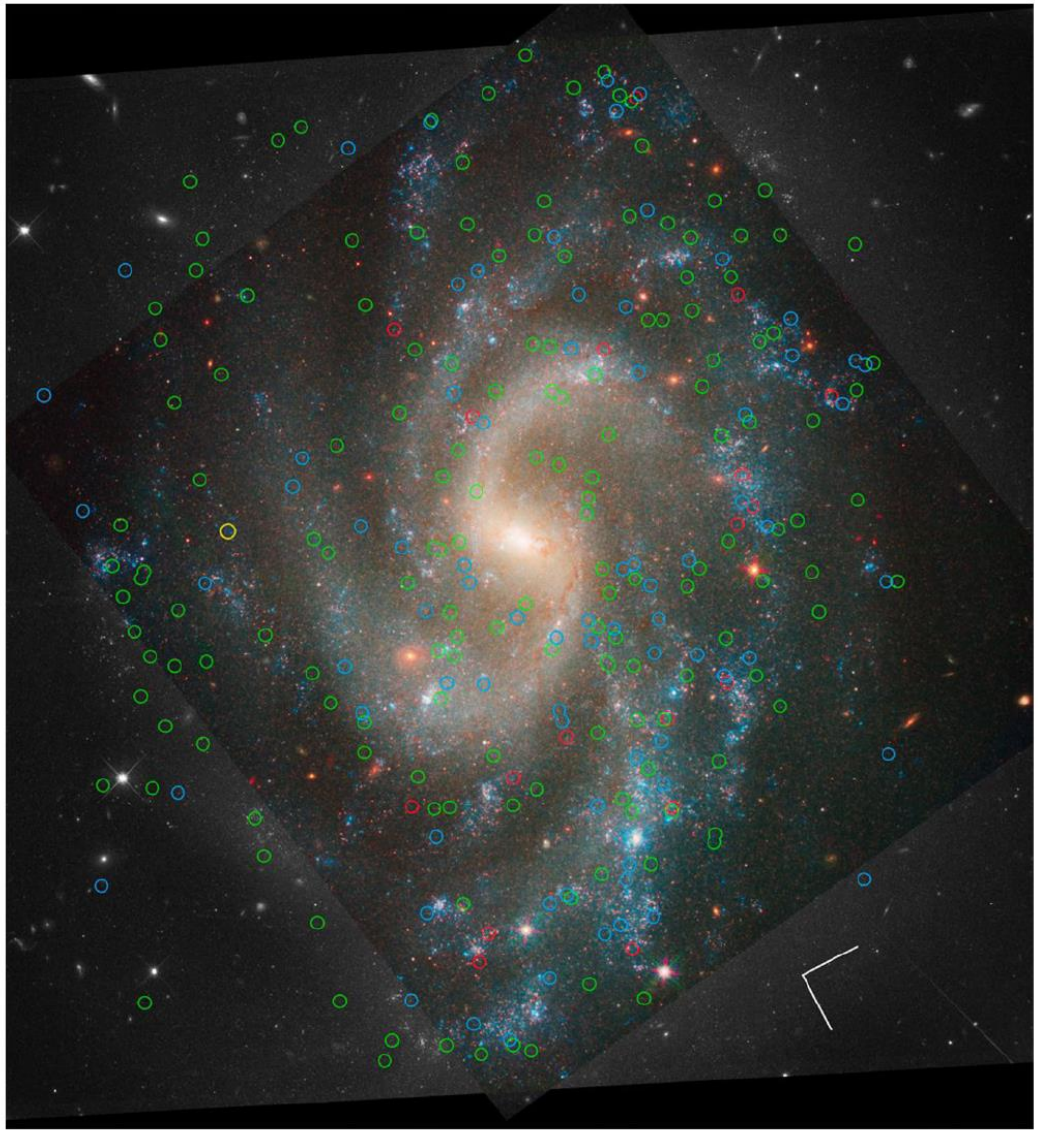

Figure 2. *HST* images of NGC 5584. The positions of Cepheids with periods in the range $P > 60$ days, 30 days $< P < 60$ days, and 10 days $< P < 30$ days are indicated by red, blue, and green circles, respectively. A yellow circle indicates the position of the host galaxy's SN Ia. The orientation is indicated by the compass rose whose vectors have lengths of 15″ and indicate north and east. The black and white regions of the images show the WFC3 optical data and the color includes the WFC3–IR data.

Riess et al. (2011)

Constante de Hubble H_0

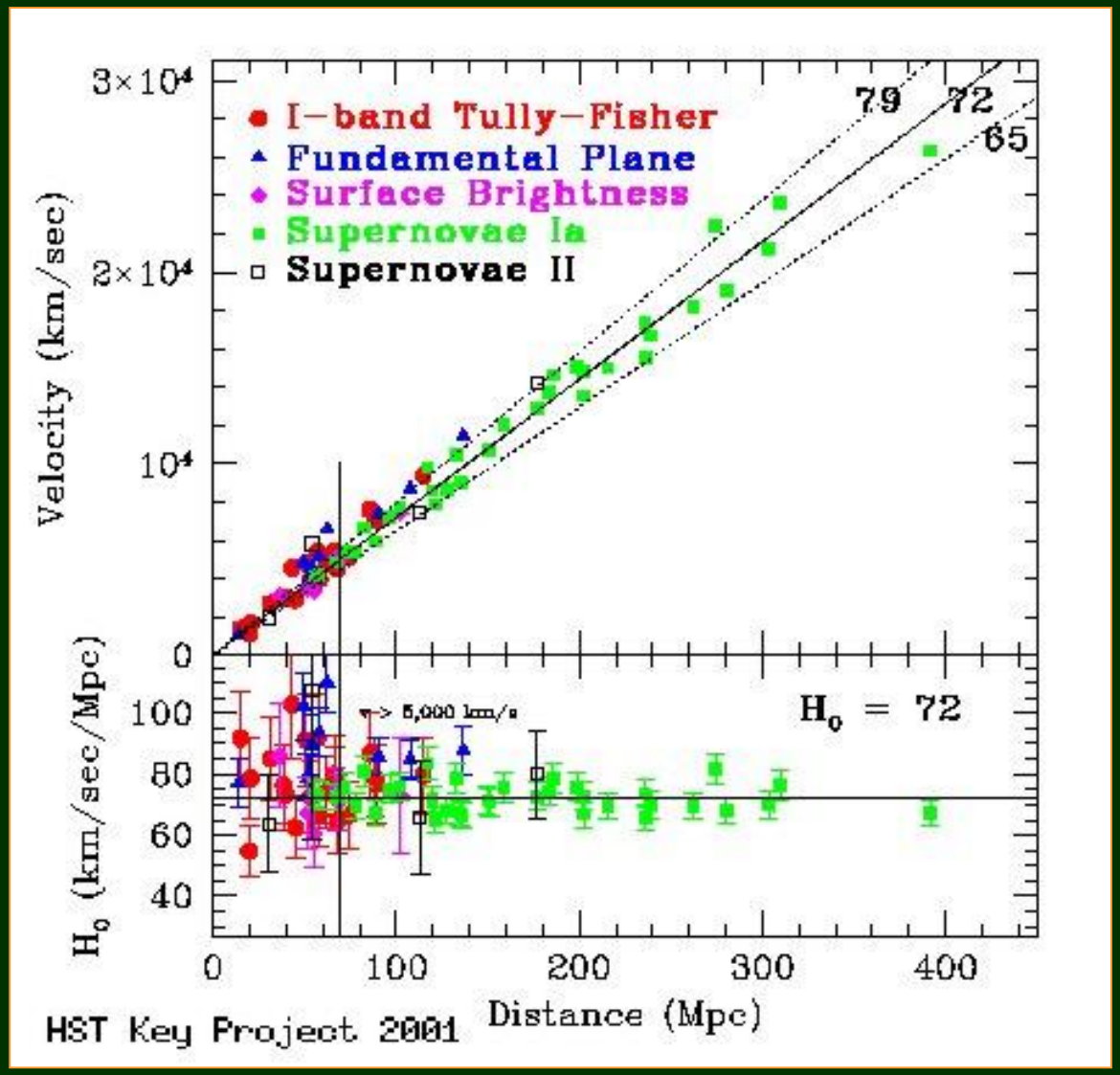

Escala de distancias completa "aproximada"

Geometry:

- MW: 15 trig. parallaxes of Cepheids
- LMC and M31: detached eclipsing binaries
- NGC 4258: water masers

Riess et al. 2016, ApJ 826, 56

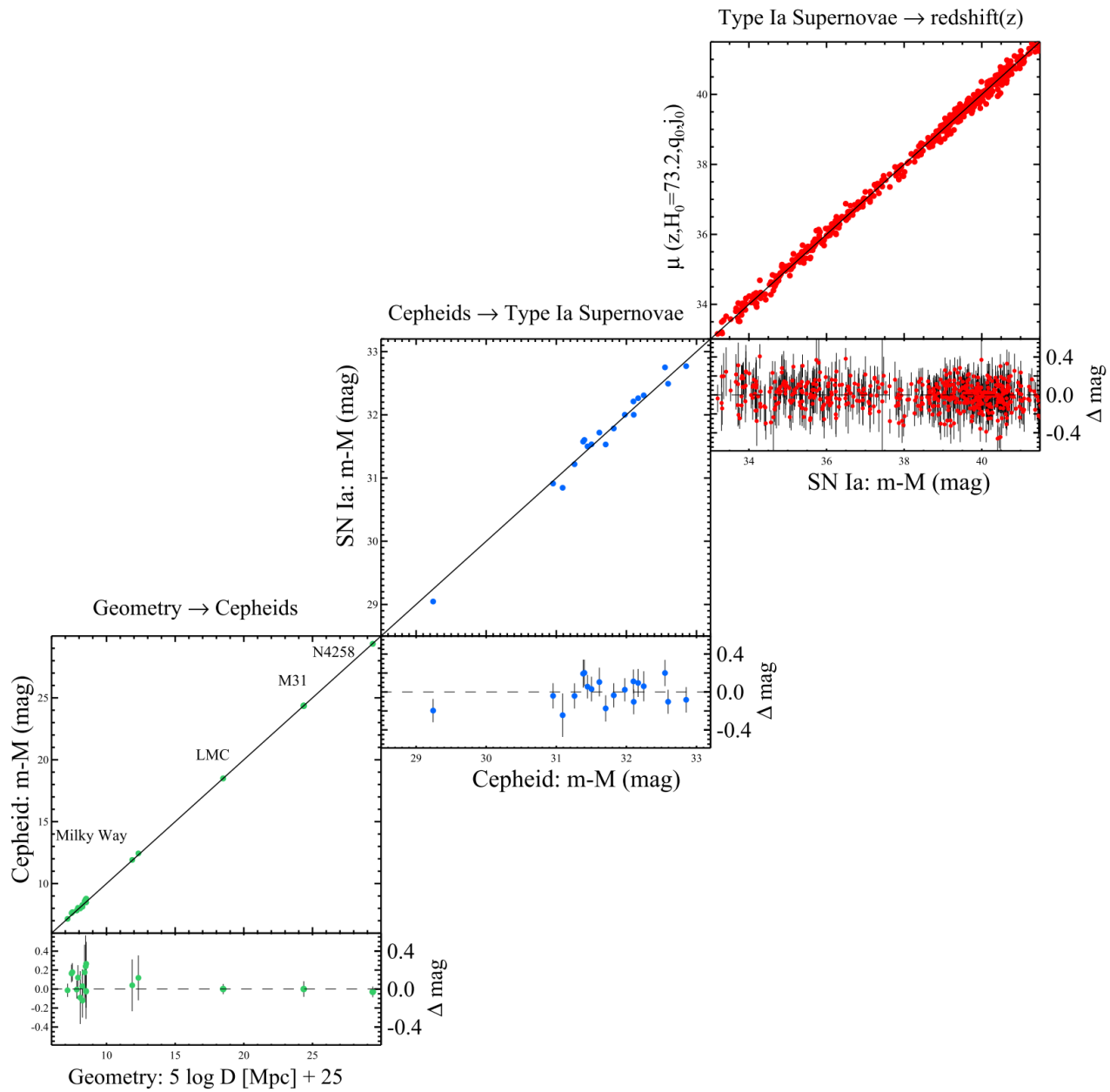

Figure 10. Complete distance ladder. The simultaneous agreement of pairs of geometric and Cepheid-based distances (lower left), Cepheid and SN Ia-based distances (middle panel) and SN and redshift-based distances provides the measurement of the Hubble constant. For each step, geometric or calibrated distances on the *x*-axis serve to calibrate a relative distance indicator on the *y*-axis through the determination of M or H_0. Results shown are an approximation to the global fit as discussed in the text.

Another Problem: Peculiar Velocities

- Note that we can in practice only observe the radial component
- Peculiar velocities act as a noise (on the $V = cz$ axis, orthogonal to errors in distances) in the Hubble diagram - and could thus bias the measurements of the H_0 (which is why we want "far field" measurements)

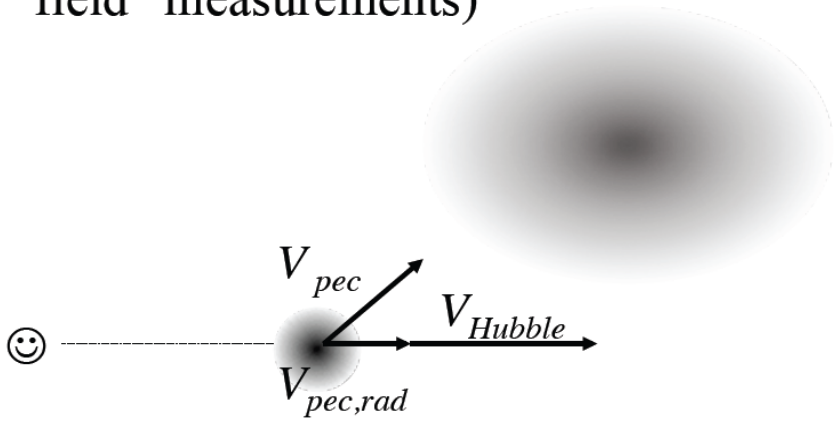

$$V_{total} = V_{Hubble} + V_{pec,rad}$$

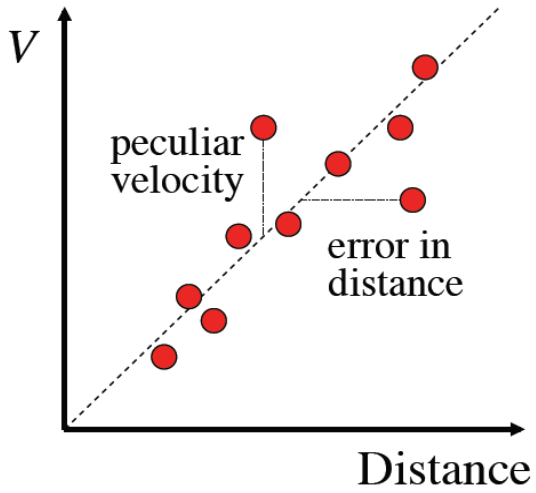

S. Djorgovski, 2013

El supercúmulo de Shapley

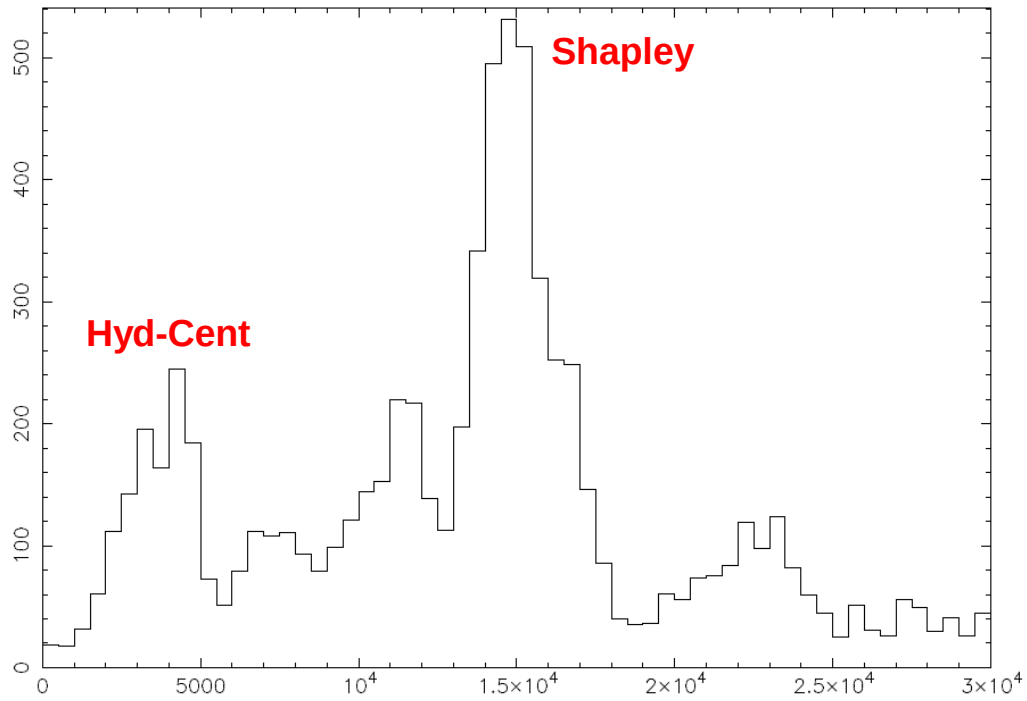

Fig. 2. Histogram of galaxy velocities in the direction of the Shapley Supercluster with all velocities available in the range $0\ \mathrm{km\,s^{-1}} \leq v \leq 30000\ \mathrm{km\,s^{-1}}$, with a step size of $500\ \mathrm{km\,s^{-1}}$.

Proust et al. 2006,
A&A 447, 133

El supercúmulo Laniakea

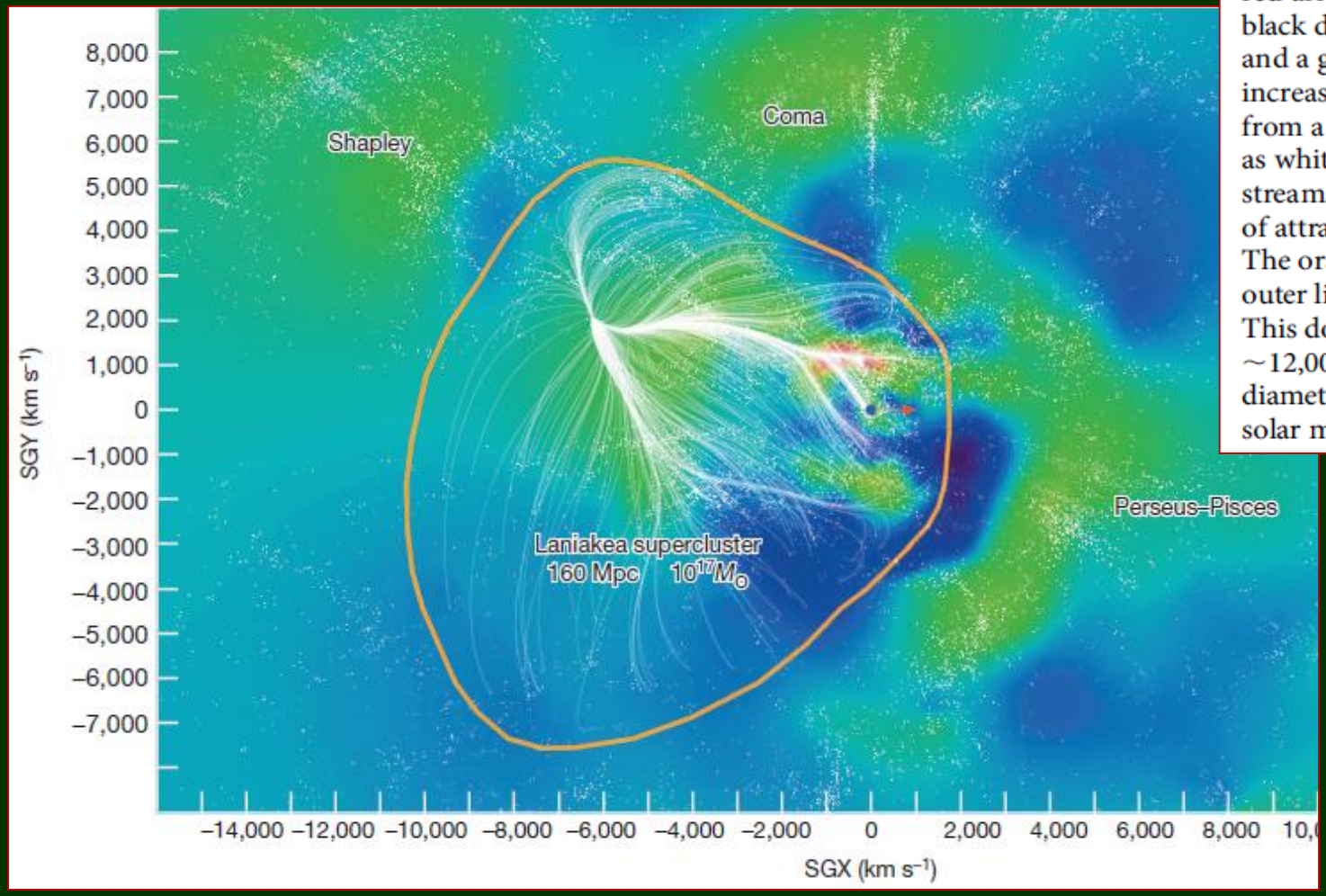

Figure 2 | A slice of the Laniakea supercluster in the supergalactic equatorial plane. Shaded contours represent density values within the equatorial slice, with red at high densities, green at intermediate densities and blue in voids. Our Milky Way galaxy is located at the black dot at the origin of the supergalactic coordinates system: a red arrow points right from the black dot toward increasing SGX and a green arrow points up toward increasing SGY. Individual galaxies from a redshift catalogue are given as white dots. Velocity flow streams within the Laniakea basin of attraction are shown in white. The orange contour encloses the outer limits of these streams. This domain has a extent of $\sim$12,000 km s^{-1}($\sim$160 Mpc diameter) and encloses $\sim 10^{17}$ solar masses, $M_\odot$.

Tully et al. 2014, Nature 513, 71